

Early diagnosis of lymph node metastasis: Importance of intranodal pressures

Yoshinobu Miura,¹ Mamoru Mikada,¹ Tomoki Ouchi,¹ Sachiko Horie,² Kazu Takeda,¹ Teppei Yamaki,¹ Maya Sakamoto,³ Shiro Mori^{1,4} and Tetsuya Kodama¹

¹Graduate School of Biomedical Engineering; ²Institute of Development, Aging and Cancer, Tohoku University, Sendai, Japan; ³Departments of Oral Diagnosis; ⁴Oral and Maxillofacial Surgery, Tohoku University Hospital, Sendai, Japan

Key words

Early diagnosis, EPR effect, intranodal pressure, lymph node metastasis, lymphatic network, mouse model of metastasis

Correspondence

Tetsuya Kodama, Laboratory of Biomedical Engineering for Cancer, Graduate School of Biomedical Engineering, Tohoku University, 4-1 Seiryō, Aoba Ward, Sendai, Miyagi 980-8575, Japan.
Tel./Fax: +81-22-717-7583;
E-mail: t.kodama@m.tohoku.ac.jp

Funding Information

Japan Society for the Promotion of Science.

Received October 10, 2015; Revised December 20, 2015;
Accepted December 23, 2015

Cancer Sci 107 (2016) 224–232

doi: 10.1111/cas.12873

Regional lymph node status is an important prognostic indicator of tumor aggressiveness. However, early diagnosis of metastasis using intranodal pressure, at a stage when lymph node size has not changed significantly, has not been investigated. Here, we use an MXH10/Mo-*lpr/lpr* mouse model of lymph node metastasis to show that intranodal pressure increases in both the subiliac lymph node and proper axillary lymph node, which are connected by lymphatic vessels, when tumor cells are injected into the subiliac lymph node to induce metastasis to the proper axillary lymph node. We found that intranodal pressure in the subiliac lymph node increased at the stage when metastasis was detected by *in vivo* bioluminescence, but when proper axillary lymph node volume (measured by high-frequency ultrasound imaging) had not increased significantly. Intravenously injected liposomes, encapsulating indocyanine green, were detected in solid tumors by *in vivo* bioluminescence, but not in the proper axillary lymph node. Basic blood vessel and lymphatic channel structures were maintained in the proper axillary lymph node, although sinus histiocytosis was detected. These results show that intranodal pressure in the proper axillary lymph node increases at early stages when metastatic tumor cells have not fully proliferated. Intranodal pressure may be a useful parameter for facilitating early diagnosis of lymph node metastasis.

The status of tumor-draining lymph nodes (LNs) is a prognostic factor for determining the cancer stage and thus treatment planning. The detection of metastasis in tumor-draining LNs has been carried out using non-invasive imaging methods, including computed tomography (CT), MRI, PET, and single photon emission CT ultrasound (US).^(1–4) Pooled estimates for sensitivity, on a per-neck basis, for CT, MRI, PET, and US are 52% (95% confidence interval, 39–65%), 65% (34–87%), 66% (47–80%), and 66% (45–77%), respectively, when used to detect cervical metastases in patients with clinically N0 head and neck cancer.⁽⁵⁾ Computed tomography, MRI, PET, and US do not differ in sensitivity and specificity, with the exception that CT shows superior specificity to US in patients with clinically N0 head and neck cancer.⁽⁵⁾ Recently developed hybrid imaging technologies (CT/MRI/US) and PET functional imaging have offered improvements,⁽⁶⁾ but additional advances are required to reduce costs and further increase sensitivity and specificity.

Intranodal pressure (INP) correlates positively with tumor volume in primary breast cancer, and has been used to predict metastasized LN size in the operating theater.⁽⁷⁾ Tumor-secreted lymphangiogenic factors and metastasis-promoting chemokines flow toward peritumoral lymphatic vessels, changing the microenvironment in draining LNs to one favoring deposition, survival, and growth of metastases.⁽⁸⁾ During these processes, alterations in blood vessel volume and density

precede changes in downstream LN size.⁽⁴⁾ Therefore, INP elevations in draining LNs may indicate metastasis.

In the absence of more clinically relevant metastasis models, studies have used xenogeneic grafts in immune deficient nude or SCID mice.^(9–11) Here, we used MXH10/Mo-*lpr/lpr* (MXH10/Mo/*lpr*) inbred mice, which develop systemic swelling of LNs that reach up to 10 mm in diameter (similar in size to human LNs).^(12–16) The basic structures of the LNs (including the medulla, paracortex, and cortex) and lymphatic channels are preserved.⁽⁴⁾

In the present study, tumor cells were injected into the subiliac LN (SiLN) to induce metastasis (through connecting lymphatic vessels) to the proper axillary LN (PALN).⁽⁴⁾ We show that INP increases in these LNs during the course of metastasis.

Materials and Methods

The Institutional Animal Care and Use Committee of Tohoku University (Sendai, Japan) approved all *in vivo* study protocols.

Cell culture. Malignant fibrous histiocytoma-like KM-Luc/GFP cells, expressing a fusion of the luciferase and enhanced-green fluorescent protein genes,⁽⁴⁾ were cultured as previously described.⁽¹⁴⁾ C3H/He mouse mammary carcinoma (FM3A-Luc) cells, expressing the luciferase gene,⁽¹²⁾ and B16F10 mouse melanoma cells (Cell Resource Center for Biomedical

Research, Institute of Development, Aging, and Cancer, Tohoku University) were maintained in RPMI-1640 medium supplemented with 10% FBS, 1% L-glutamine–penicillin–streptomycin, and 1 mg/mL G418 (Sigma-Aldrich, St. Louis, MO, USA). Cell lines were incubated (37°C, 5% CO₂/95% air) until 80% confluence was achieved. Lack of *Mycoplasma* contamination was confirmed on the inoculation day (MycAlert *Mycoplasma* Detection Kit; Lonza Rockland, Allendale, NJ, USA).

Polymerase chain reaction analysis of vascular endothelial growth factor family expression. Expression of vascular endothelial growth factor (VEGF)-A, VEGF-B, VEGF-C, and VEGF-D in KM-Luc/GFP and FM3A-Luc cells was examined. B16F10 cells were used as the positive control for VEGF-C expression. RNA was extracted (RNeasy Mini Plus kit; Qiagen, Düsseldorf, Germany), and isolated RNA (1 µg) was reverse-transcribed with ReverTra Ace (Toyobo, Osaka, Japan). Polymerase chain reaction was carried out with GoTaq Hot Start Master Mix (Promega, Madison, WI, USA). The negative control used sterile distilled water. Table S1 shows the PCR primers used.

Mice. MXH10/Mo/lpr mice (weight, 27–37 g; 14–16 weeks old) were maintained at the Institute for Animal Experimentation, Graduate School of Medicine, Tohoku University.

Induction of metastasis to PALN. Cells, 2.0×10^4 KM-Luc/GFP or 2.0×10^4 FM3A-Luc cells in 60 µL vehicle (20 µL PBS plus 40 µL of 400 mg/mL Matrigel; Collaborative Biomedical Products, Bedford, MA, USA) were injected into the SiLNs of mice anesthetized with 2% isoflurane in oxygen (Abbott, Lake Forest, IL, USA). In controls, 60 µL vehicle was injected (Figs. 1A and 1B). Inoculation (24-gauge needle) was guided by high-frequency US imaging (VEVO770; VisualSonics, Toronto, ON, Canada) using a 25-MHz transducer (RMV-710B; VisualSonics) (Fig. 1C).⁽¹⁷⁾ The inoculation day was defined as day 0. Three groups were used for evaluation of tumor growth/metastasis, PALN size, and INP: control, KM-Luc/GFP, and FM3A-Luc (Fig. 1A). The KM-Luc/GFP group was divided into two subgroups (day 3 and day 6), and the FM3A-Luc group into three subgroups (day 6, day 10, and day 14).

Induction of solid tumor. Solid tumor was produced by s.c. injection of 2.0×10^4 KM-Luc/GFP or 2.0×10^4 FM3A-Luc cells (suspended in 60 µL PBS/Matrigel vehicle) into the right or left flank of the mouse.

Detection of tumor growth and metastasis. Metastasis to the PALN was assessed using *in vivo* bioluminescence imaging (IVIS; Xenogen, Waltham, MA, USA) on days 0, 3, and 6 for KM-Luc/GFP cells, and days 0, 3, 6, 10, and 14 for FM3A-Luc cells.^(4,18) Metastasis was considered successful when PALN luciferase activity exceeded the background level in controls ($\sim 4 \times 10^4$ photons/s). Solid tumors were assessed by IVIS at the same time points.

Measurement of INP in SiLN and PALN. The mouse was anesthetized and an arc-shaped incision made in the abdominal skin from the SiLN to the PALN (Fig. 1B). As indocyanine green (ICG) injected into the SiLN seldom flowed across the midline to the contralateral side and always flowed from the SiLN to the PALN, it is unlikely that surgery damaged the lymphatic vessels connecting the SiLN and PALN or influenced INP measurements. A 21-gauge hypodermic needle was connected to a pressure transducer (BLPR2; World Precision Instruments, Sarasota, FL, USA) through a three-way stopcock (Terumo, Tokyo, Japan) filled with physiological saline. The pressure transducer was connected to a directly coupled ampli-

fier system (Bridge8; World Precision Instruments) linked to a computer running analysis software (LabScribe2; iWorx Systems, Dover, NH, USA). A zero reading was obtained with the needle open to the air at the level of the node to be measured.⁽¹⁹⁾ Intranodal pressure was measured (0.02 s sampling rate) with the needle inserted for 5 min into the central region of the LN.

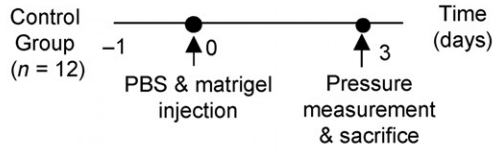
Measurement of PALN and solid tumor volume. Proper axillary LN volume was measured using high-frequency US imaging (VEVO770) with a 25-MHz transducer (RMV-710B), on days -1 (before inoculation), 2, and 5 for KM-Luc/GFP cells, and days -1, 2, 5, 9, and 13 for FM3A-Luc cells.⁽⁴⁾ Solid tumor volume was calculated from digital caliper measurements as: $\pi/6 \times \text{width}^2 \times \text{length}$.

Production of ICG liposomes. 1,2-Distearoyl-sn-glycero-3-phosphatidylcholine (MC8080; NOF, Tokyo, Japan) and 1,2-distearoyl-sn-glycerol-3-phosphatidylethanolamine-methoxy-PEG (DSPE-PEG[2000-OMe]) (DSPE-020CN, NOF; 94:6 mol/mol) were dissolved in chloroform. Following solvent removal (flask rotation, 60 hPa, 65°C, 2 h), the liposome film was dissolved in 80 µM ICG (in PBS). Following several freeze–thaw cycles to form large unilamellar vesicles, ICG liposome diameter was adjusted to <200 nm using extruding equipment (Northern Lipids, Burnaby, Canada) and sizing filters (100, 200, and 600 nm pores). Unencapsulated ICG was removed by PD-10 columns (GE Healthcare, Little Chalfont, UK). After sterilization (0.45-µm pore filter; Millipore, Billerica, MA, USA), the lipid concentration (Phospholipid C-test; Wako Pure Chemical Industries, Osaka, Japan) was adjusted to 0.5 mg/mL. The ICG liposome zeta potential and size were -2.2 mV and 134.7 ± 9.39 nm (mean \pm SD, $n = 2$), respectively (ELSZ-2; Otsuka Electronics, Osaka, Japan). Light absorption characteristics were measured with a spectrum analyzer (UV2600; Shimadzu, Kyoto, Japan). To confirm ICG liposome stability at mammalian body temperature, 1 mL aliquots was incubated at 37°C. Any ICG released was removed by PD-10 columns, and absorbance at 800 nm (to detect any remaining ICG) measured after 0 min, 5 min, 1 h, 6 h, and 24 h (SpectraMax M2/M2e multidetection microplate reader; Molecular Devices, Sunnyvale, CA, USA). Approximately 20% of the ICG liposomes had collapsed after 48 h at 37°C.

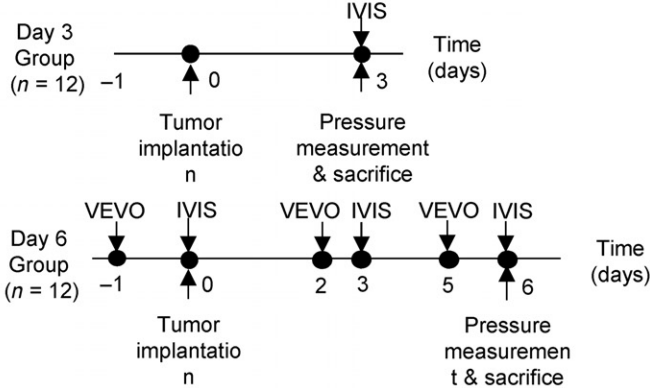
Leakage of ICG liposomes from vasculature. Indocyanine green liposome leakage from SiLN and PALN vasculature was measured by IVIS, with solid tumors used as a positive control. Indocyanine green liposomes were injected i.v. on day 6 (KM-Luc/GFP) or 14 (FM3A-Luc) after cell inoculation, and leakage measured 24 h after injection. The mouse was then killed, and the harvested SiLN, PALN, and solid tumor tissues weighed and homogenized in 1 mL PBS (T25 Basic Ultra-Turrax S1; IKA Works, Staufen, Germany). The fluorescence intensity of supernatant in 48-well plates (500 µL/well) was measured by IVIS.

Histological analysis. The LNs were excised from the mice after IFP measurements had been made. Some LNs were fixed overnight in 10% formalin at 4°C, dehydrated, embedded in paraffin, serially sectioned (3–5 µm), and either stained with H&E or immunostained for LYVE-1-positive, CD31-positive cells (Discovery XT Automated Staining Processor; Ventana Medical Systems, Tucson, AZ, USA).⁽⁴⁾ Immunostaining of lymphatic endothelial cells was carried out using polyclonal rabbit anti-mouse LYVE-1 antibody (4 µg/mL, 2 h at room temperature) (103-PA50AG; Cosmo Bio, Tokyo, Japan) in combination with biotinylated anti-rabbit IgG (20 min at room temperature; Vector Laboratories, Burlingame, CA, USA) and

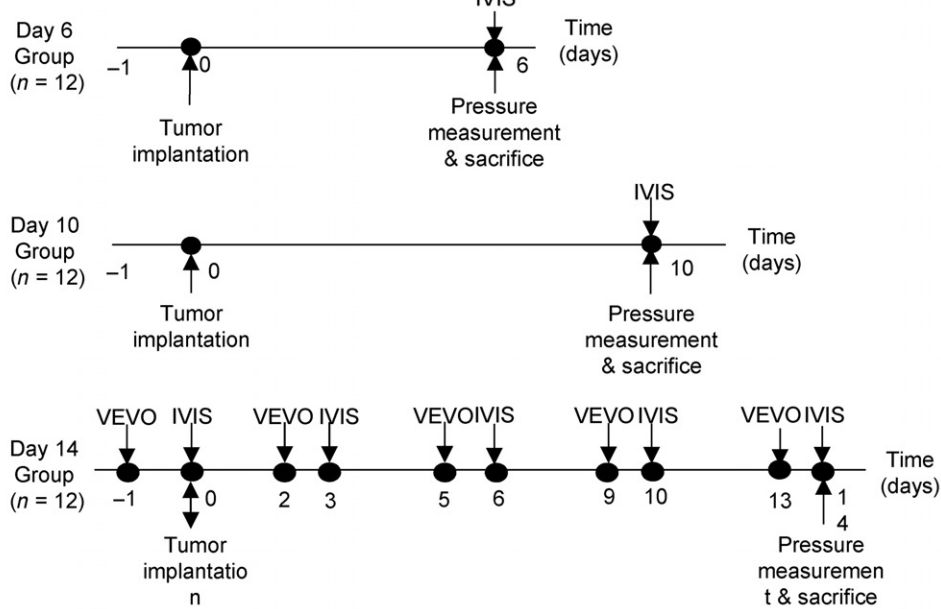
A (i) Control



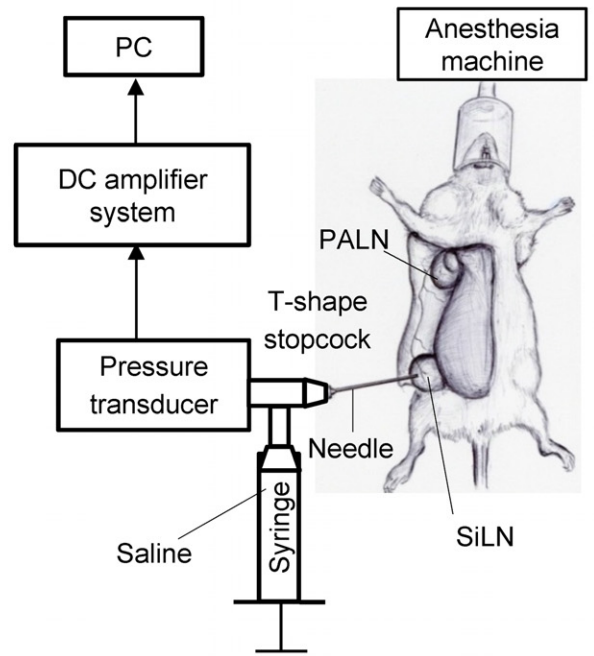
(ii) KM-Luc/GFP



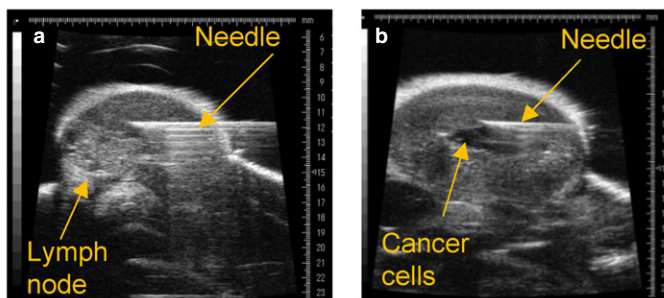
(iii) FM3A-Luc



B



C



D

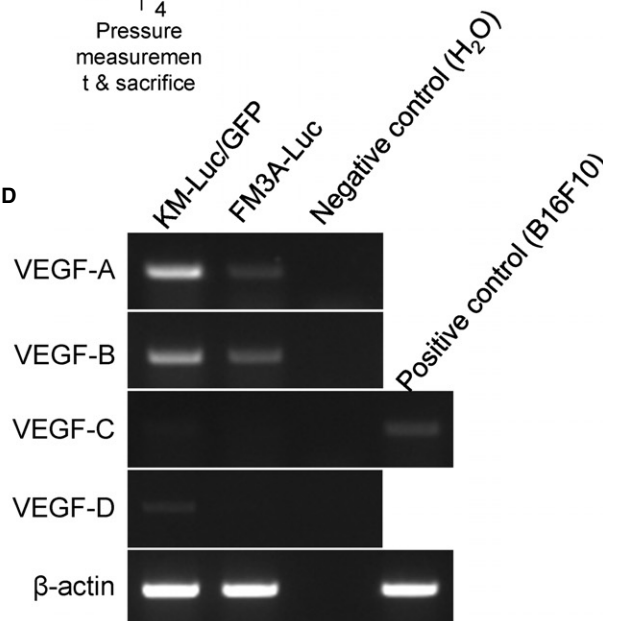
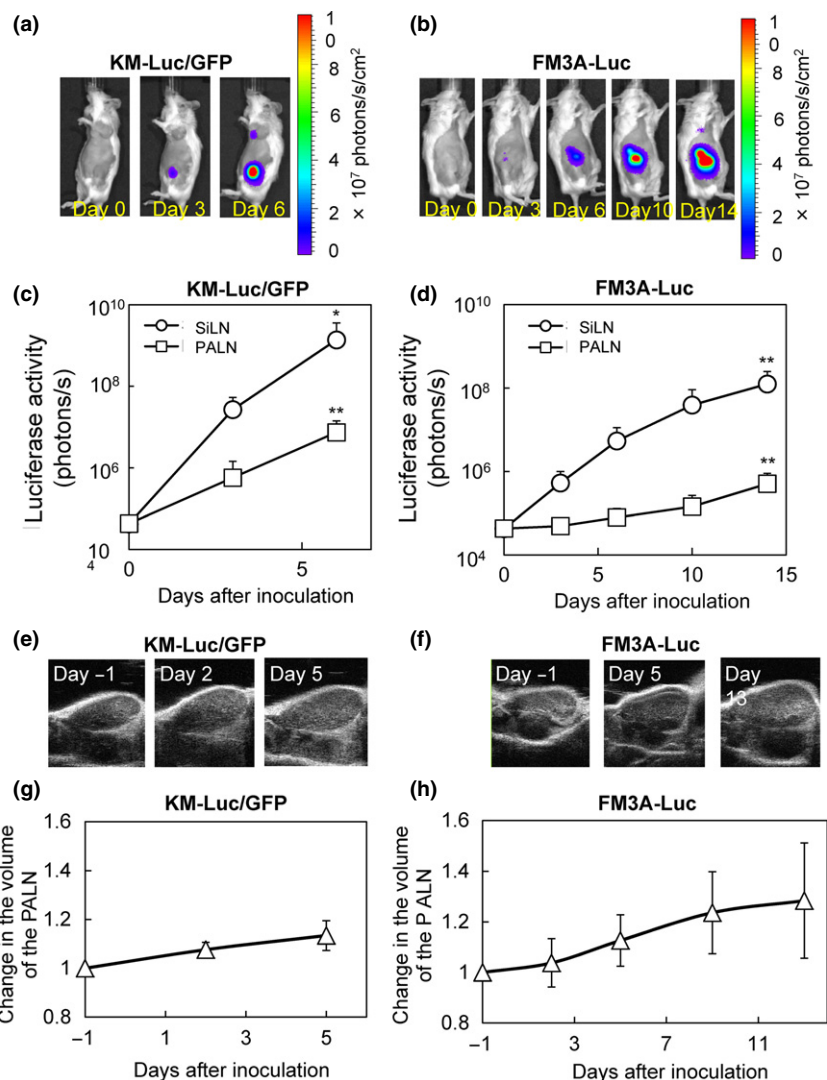


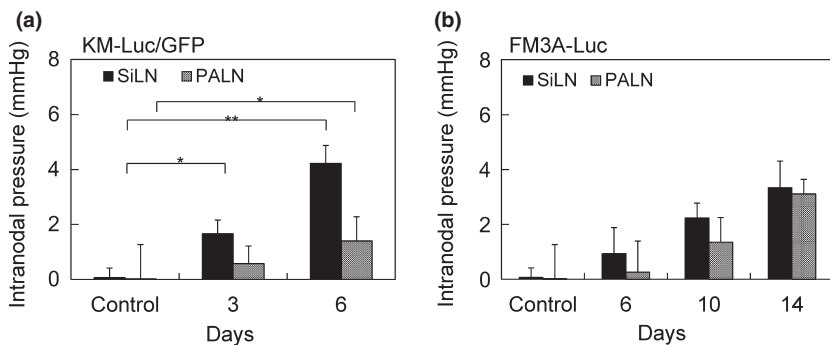
Fig. 1. Tumor cell inoculation into the subiliac lymph node (SiLN) and cell characteristics. (A) Experimental schedule. The 72 mice included in the analysis were divided into three groups: control ($n = 12$), KM-Luc/GFP ($n = 24$), and FM3A-Luc ($n = 36$). The day of inoculation was defined as day 0. The KM-Luc/GFP group was divided into two subgroups: day 3 and day 6 ($n = 12$, each subgroup). The FM3A-Luc group was divided into three subgroups: day 6, day 10, and day 14 ($n = 12$, each subgroup). IVIS, *in vivo* luminescence imaging system; VEO, high-frequency ultrasound imaging system. (B) Intranodal pressure measurement. A hypodermic needle, connected to a pressure transducer, was inserted into the central region of the SiLN or PALN for 5 min. (C) Needle location in the SiLN before (a) and immediately after (b) inoculation. Cells were detected as a central shadow. Images were obtained with VEO. (D) RNA isolation and PCR to detect the expression of the vascular endothelial growth factor (VEGF) family. Gel electrophoretic analysis of PCR for the VEGF family in KM-Luc/GFP and FM3A-Luc cells. Sterile distilled water was used for the negative control. B16F10 cells, which express VEGF-C, were used as a positive control for VEGF-C.



diaminobenzidine. Immunostaining of vascular endothelial cells was achieved using pre-diluted polyclonal goat anti-CD31 antibody (1:100 dilution; 2 h at room temperature) (sc-1506; Santa Cruz Biotechnology, Dallas, TX, USA) in combination with biotinylated anti-goat IgG (20 min at room temperature; Vector Laboratories) and diaminobenzidine. The remaining LN specimens were prepared as frozen sections (10- μ m slices), to detect the area of CD31-positive cells using immunofluorescence. Sections were fixed in 4% paraformaldehyde (15 min at room temperature), washed (PBS), incubated overnight at 4°C with purified rat anti-mouse CD31 primary antibody (1:100 in PBS with 3% BSA and 0.1% Triton-X; 553370, BD Pharmingen, San Diego, CA, USA), washed (PBS), incubated (40 min, 4°C) with Alexa 555-conjugated

goat anti-rat secondary antibody (1:500; Life Technologies, Carlsbad, CA, USA), washed (PBS), and mounted with Vectashield (Vector Laboratories).⁽²⁰⁾ Histological images were captured using a fluorescence microscope (BX51; Olympus, Tokyo, Japan) and digital camera (DP72; Olympus). The red channel from each RGB image was exported into Photoshop CS3 (Adobe Systems, San Jose, CA, USA). To measure vessel density in each section, the five most vascularized fields (hot-spot areas) were selected under low magnification ($\times 40$ or $\times 100$), and the percentage of each field stained for CD31 calculated ($\times 200$) using ImageJ software (NIH).⁽⁴⁾

Statistical analysis. Data are presented as mean \pm SD or mean \pm SEM. Differences between groups were determined by one-way or two-way ANOVA followed by Tukey's test or



KM-Luc/GFP	Control (mmHg)		Day 3 (mmHg)		Day 6 (mmHg)	
	SiLN	PALN	SiLN	PALN	SiLN	PALN
Mean	0.07	0.02	1.66	0.57	4.22	1.41
SEM	0.34	1.24	0.45	0.65	0.66	0.88

FM3A-Luc	Control (mmHg)		Day 6 (mmHg)		Day 10 (mmHg)		Day 14 (mmHg)	
	SiLN	PALN	SiLN	PALN	SiLN	PALN	SiLN	PALN
Mean	0.07	0.02	0.93	0.26	2.23	1.36	3.34	3.11
SEM	0.34	1.24	0.95	1.13	0.54	0.90	0.96	0.53

Fig. 3. Intranodal pressure (INP) measurements in the subiliac lymph node (SiLN), and proper axillary lymph node (PALN). (A) KM-Luc/GFP cells (SiLN and PALN, $n = 36$). * $P < 0.05$ for SiLN group versus control on day 3; ** $P < 0.01$ for SiLN versus control on day 6; * $P < 0.05$ for PALN versus control on day 6 (two-way ANOVA and Tukey's test). (B) FM3A-Luc cells (SiLN and PALN, $n = 36$). There were no significant changes in INP in the PALN. Mean \pm SEM values are shown.

Student's *t*-test (GraphPad Prism 6J, La Jolla, CA, USA). $P < 0.05$ was considered statistically significant.

Results

Induction of metastasis to PALN. KM-Luc/GFP or FM3A-Luc cells were injected into the SiLN to provoke metastasis to the PALN. Both cell types expressed VEGF-A and VEGF-B but not VEGF-C; KM-Luc/GFP but not FM3A-Luc cells showed slight VEGF-D expression (Fig. 1D). Figure 2 shows the luciferase activity of KM-Luc/GFP cells in the SiLN and PALN (days 0, 3, and 6; Fig. 2A,C), and that of FM3A-Luc cells (days 0, 3, 6, 10, and 14; Fig. 2B,D). Luciferase activity in both LNs increased over time, with larger increases in the SiLN. Tumor cells were detected in the PALN on day 6 for KM-Luc/GFP cells and day 14 for FM3A-Luc cells. In subsequent experiments, INP measurements were made from the early stages of metastasis to day 6 (KM-Luc/GFP) or day 14 (FM3A-Luc).

Changes in PALN volume. Lymph node size is an important variable used for US diagnosis of LN metastasis.^(4,21) Next, we measured changes in PALN volume using 3D high-frequency US imaging; data are shown for KM-Luc/GFP cells (Fig. 2E,G) and FM3A-Luc cells (Fig. 2F,H). Proper axillary LN volume was normalized to that on day -1 . There were no significant changes in PALN volume over time for either cell type, supporting a previous finding that evaluation of LN size is not sufficient for early diagnosis of LN metastasis.⁽⁴⁾

Intranodal pressure in SiLN and PALN. Next, we investigated temporal changes in the INP in the SiLN and PALN (Fig. 3).

In control (i.e., non-treated) mice, INP was higher in the SiLN than in the PALN (0.07 ± 0.34 mmHg vs 0.02 ± 1.24 mmHg, $n = 36$), indicating a pressure gradient between these LNs. For KM-Luc/GFP cells, INP increased over time in both the SiLN (Fig. 3A; $n = 24$; $P < 0.05$, SiLN versus control on day 3; $P < 0.01$, SiLN versus control on day 6) and PALN (Fig. 3A; $n = 24$; $P < 0.05$, PALN versus control on day 6). Intranodal pressure in the SiLN and PALN appeared to increase over time for FM3A-Luc cells (Fig. 3A), but the changes were not significant.

Indocyanine green liposome leakage from vasculature. Angiogenesis, a hallmark of cancer,^(22,23) leads to immature, hyper-permeable tumor vessels and an elevation of interstitial fluid pressure in a solid tumor. To examine the enhanced permeability and retention (EPR) effect⁽²⁴⁾ during the early stages of LN metastasis, we injected ICG liposomes i.v. and compared their leakages from the SiLN, PALN, and solid tumor. For the KM-Luc/GFP group at day 6, the average sizes of the solid tumor, SiLN, and PALN were 182.81 ± 49.15 mm³ ($n = 5$), 358.76 ± 73.69 mm³ ($n = 5$), and 195.49 ± 34.78 mm³ ($n = 5$), respectively. For the FM3A-Luc group at day 14, the average sizes of the solid tumor, SiLN, and PALN were 165.18 ± 87.74 mm³ ($n = 5$), 411.41 ± 33.00 mm³ ($n = 5$), and 157.90 ± 27.45 mm³ ($n = 5$), respectively. There were no significant differences in LN size between the KM-Luc/GFP and FM3A-Luc groups (one-way ANOVA). First, we used *in vivo* bioluminescence imaging to confirm solid tumor growth (Fig. 4A(i),B(i)) and metastasis progression (Fig. 4A(iii),B(iii)). Twenty four hours after injection, ICG liposomes were detected around the solid tumor (Fig. 4A(ii),B(ii)), but did not accumulate in the SiLN and PALN (Fig. 4A(iv),B(iv)).

Fig. 4. Leakage of indocyanine green (ICG) liposomes. Bioluminescence and fluorescence images of mice inoculated with KM-Luc/GFP (A,C,E) or FM3A-Luc (B,D,F) cells. Representative bioluminescence images: A(i), A(iii), B(i), and B(iii). Representative fluorescence images: A(ii), A(iv), B(ii), and B(iv). Solid tumor groups: A(i), A(ii), B(i), and B(ii). Metastasis groups: A(iii), A(iv), B(iii), and B(iv). Bioluminescence images were obtained 6 days after inoculation of KM-Luc/GFP cells, and 14 days after inoculation of FM3A-Luc cells. ICG liposomes were then injected i.v., and fluorescence images obtained 24 h later, that is, days 7 and 15 after inoculation of KM-Luc/GFP and FM3A-Luc cells, respectively. Quantification of luciferase activity (averaged values): KM-Luc/GFP (C) and FM3A-Luc (D). Luciferase activities were obtained 6 days after inoculation of KM-Luc/GFP cells (** $P < 0.01$, solid tumor versus proper axillary lymph node [PALN]), and 14 days after inoculation of FM3A-Luc cells (** $P < 0.01$, solid tumor versus PALN). E(i), E(ii), F(i), and F(ii): Following imaging, the subiliac lymph node (SiLN), PALN, and solid tumor were homogenized, and the fluorescence intensity of the supernatant measured by IVIS. E(i), F(i): Fluorescence images of individual wells of a 48-well plate. E(ii), F(ii): Averaged values for the fluorescence/weight ratio. Mean \pm SEM values are shown. ** $P < 0.01$ versus solid tumor (one-way ANOVA and Tukey's test).

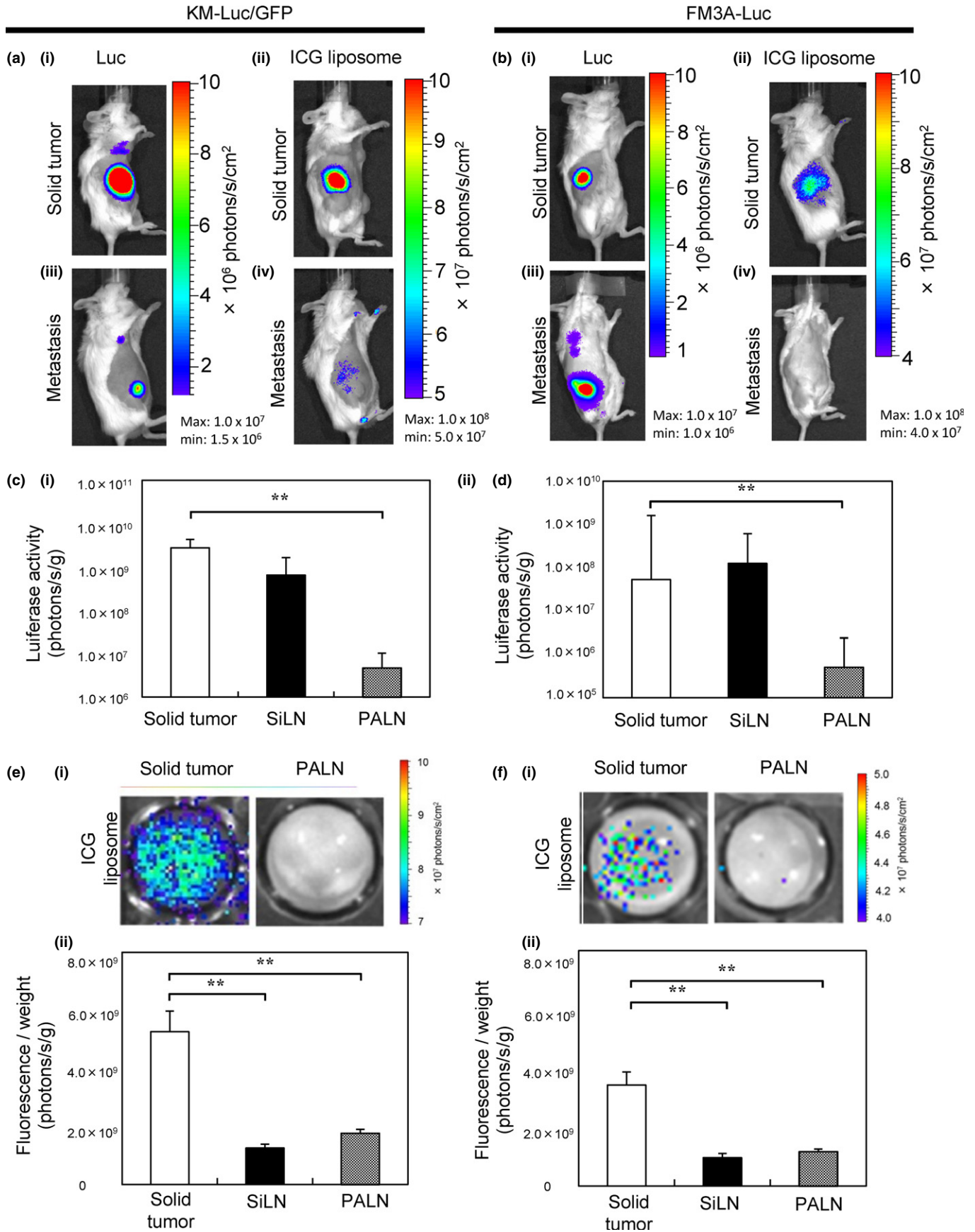


Figure 4(C,D) shows the luciferase activities of solid tumor (Fig. 4A(i),B(i)), SiLN, and PALN (Fig. 4A(iii),B(iii)). There were no significant differences in luciferase activities between solid tumor and SiLN (a site of tumor injection), whereas the luciferase activity of the solid tumor was significantly higher than that of the PALN (a site of metastasis) ($P < 0.01$, solid tumor versus PALN). Measurement of fluorescence / weight ratios in homogenized tissues revealed significant differences between solid tumor, SiLN, and PALN (Fig. 4E,F; $P < 0.01$, versus solid tumor). Thus, under the present conditions, the EPR effect that accompanies angiogenesis in solid tumors was not detected in the SiLN or PALN.

Histological findings. Figure 5 shows representative images of the SiLN and PALN stained with H&E, anti-LYVE-1 antibody, or anti-CD31 antibody, under control conditions (day 3), or after inoculation with KM-Luc/GFP (day 6) or FM3A-Luc (day 14) cells. The basic internal structures (medulla, paracortex, cortex, and lymphatic channels) were preserved in tumor-containing SiLN and metastasized PALN.⁽⁴⁾ Discrete blood vessels were observed in all LNs (Fig. 5A), and lymphatic sinus histiocytosis in the PALN and SiLN (Fig. 5B). Next, we measured LN vessel density (the CD31-positive area) using immunofluorescence techniques (Fig. 6A). Blood vessel den-

sity did not differ between the control and metastasis groups (Fig. 6B,C). It has been noted that as mice age, their lymph node structures change over a period of several weeks. After 12 weeks, follicles tend to atrophy due to the accumulation of abnormal lymphocytes. We observed that the degree of atrophy was similar for control and metastatic lymph nodes, except for the portion of the lymph node comprising metastatic tumor.

Discussion

The present study demonstrates that INP measurement can detect tumor growth in a metastatic LN earlier than a volume-based evaluation using US imaging. The detection sensitivity of INP was similar to that of *in vivo* bioluminescence imaging (Figs 2,3).

In our experimental system, tumor cells were injected into the SiLN to induce metastasis to the PALN through lymphatic vessels. However, some of the tumor cells may have reached the lung by way of the thoracoepigastric vein.^(14,15) Intranodal pressure increased in both LNs over time, but was greater in the SiLN. Accumulation of ICG liposomes due to the EPR effect⁽²⁵⁾ was observed only in solid tumor after

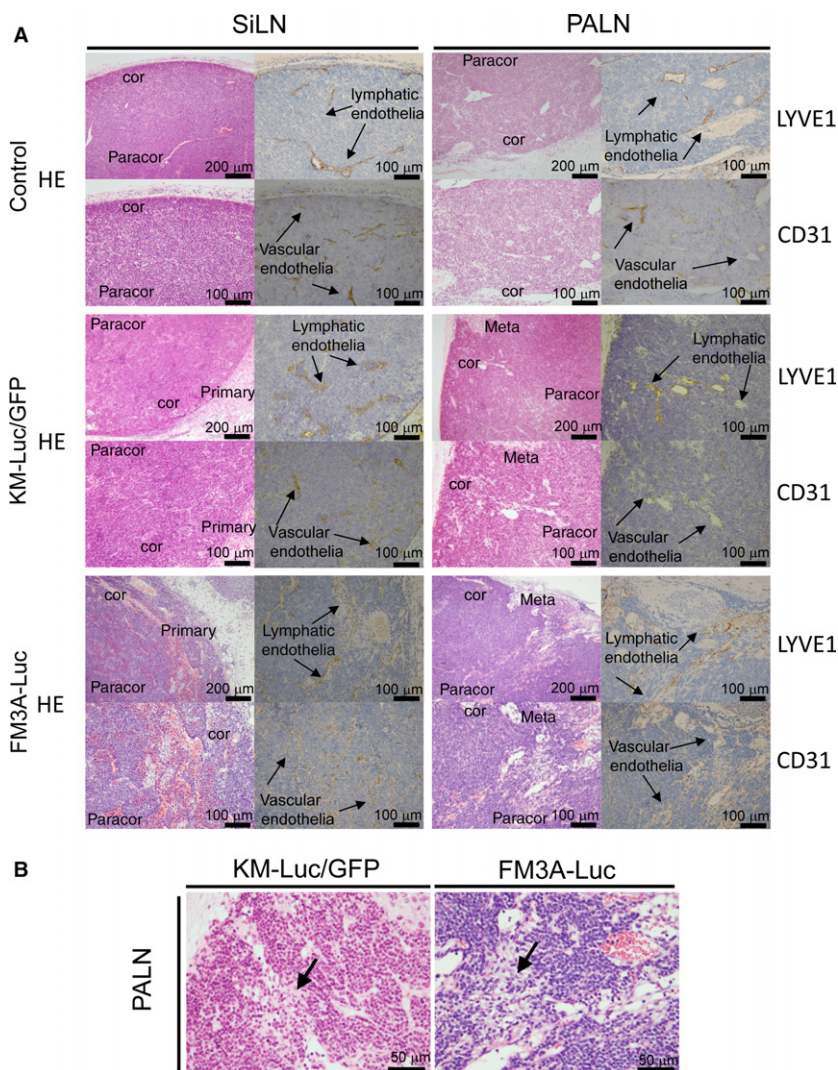


Fig. 5. Representative histological images showing the internal structures of the subiliac lymph node (SiLN) and proper axillary lymph node (PALN) after initiation of metastasis. (A) Representative images of the SiLN and PALN stained with H&E, anti-LYVE-1 antibody, or anti-CD31 antibody, under control conditions ($n = 4$) on day 3, or after inoculation with KM-Luc/GFP cells ($n = 4$) on day 6 or FM3A-Luc cells ($n = 4$) on day 14. In both the control and metastasis groups, the blood vessels remained discretely distributed. Cor, cortex; Paracor, paracortex; Meta, metastasis. (B) H&E staining of tumor-containing PALN. Histiocytosis was evident in/around the lymphatic sinus (arrows). Bar = 50 μm.

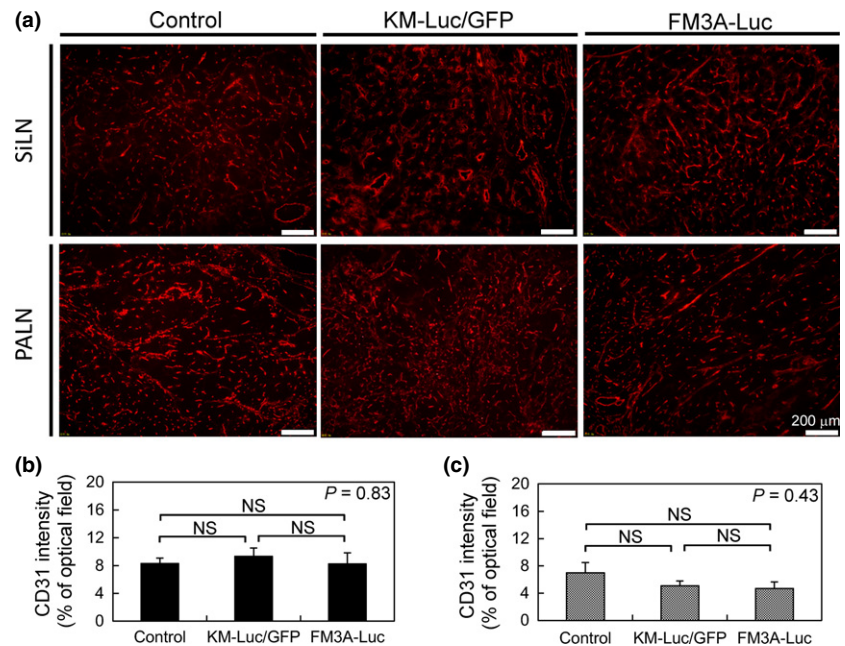


Fig. 6. Evaluation of subiliac lymph node (SiLN) and proper axillary lymph node (PALN) blood vessel density after initiation of metastasis. (A) Representative immunofluorescence images of the SiLN and PALN under control conditions ($n = 4$) on day 3 or after inoculation with KM-Luc/GFP cells ($n = 4$) on day 6 or FM3A-Luc cells ($n = 4$) on day 14, showing staining for CD31 as a marker of blood vessels. Bar = 200 μ m. (B,C) Mean values for the percentage CD31-positive area in the SiLN (B) and PALN (C). There were no significant differences in the entire lymph node blood vessel density between the control and metastasis groups (one-way ANOVA). Mean \pm SEM values are shown. NS, not significant.

24 h. Furthermore, the blood and lymphatic vessels of the SiLN and PALN showed no significant structural changes, except for sinus histiocytosis (Fig. 5). In addition, immunohistochemical studies identified no obvious neovascularity in the interstitium of either LN (Figs 5,6). As a LN is a closed space containing a vascular network that is covered by a capsule, tumor cells may grow without aggressive angiogenesis, causing INP to increase without a change in LN volume.

Most previous investigations using cells stably expressing the *VEGF-C* gene or transfection of VEGF-C have evaluated lymphatic vessel density after several weeks.^(26,27) Therefore, it is unlikely that VEGF-C would affect the increase in INP that occurred after only a few days in our study, which used tumor cells that do not express VEGF-C (Fig. 1D).

In controls, INP was higher in the SiLN than in the PALN. In the anatomical chart of a mouse,⁽¹⁴⁾ the efferent lymphatic vessel of the PALN is connected with the subclavian vein, and that of the SiLN with the PALN. The thoracoepigastric vein, which connects the subclavian vein and inferior vena cava, runs adjacent to the SiLN and PALN, and receives venous blood from these LNs through small branches. Thus, it is not surprising that INP is lower in the PALN than in the SiLN.

Bouta *et al.*⁽²⁸⁾ measured INP in the popliteal LN of TNF-Tg mice and their wild-type littermates (aged 4–10 months), and determined INP in wild-type mice to be 5.01 ± 0.41 mmHg. The difference between their value and ours may reflect the different strains of mice used and/or the

anatomical location of the LN measured. Nathanson *et al.*⁽¹⁹⁾ reported that metastasis to an axillary sentinel LN in breast cancer was associated with higher INP than that in tumor-free LNs, and that clinical suspicion of metastasis correlated with INP in predicting macrometastases.⁽⁷⁾ We expect that INP may be an important parameter for detecting the early stages of LN metastasis, when LN size has not changed significantly.

In conclusion, the present study describes for the first time temporal changes in the INP of LNs connected by a lymphatic network, after the initiation of metastasis. Downstream LN INP increases at stages when metastatic tumor cells have not fully proliferated. Thus, INP may be a useful parameter for the early diagnosis of LN metastasis.

Acknowledgments

The authors thank M. Nose for helpful discussions and the Biomedical Research Core of Tohoku University Graduate School of Medicine for technical support. The study was supported in part by Kakenhi grant numbers 26293425 (S.M.), 26670856 (S.M.), 25293382 (M.S.), 24659834 (M.S.), 26242051 (T.K.), and 24650286 (T.K.) from the Japan Society for the Promotion of Science.

Disclosure Statement

The authors have no conflict of interest.

References

- Huang X, Zhang F, Lee S *et al.* Long-term multimodal imaging of tumor draining sentinel lymph nodes using mesoporous silica-based nanoprobe. *Biomaterials* 2012; **33**: 4370–8.
- Mumprecht V, Honer M, Vigl B *et al.* In vivo imaging of inflammation- and tumor-induced lymph node lymphangiogenesis by immuno-positron emission tomography. *Cancer Res* 2010; **70**: 8842–51.
- Seo Y, Aparici CM, Chen CP *et al.* Mapping of lymphatic drainage from the prostate using filtered 99mTc-sulfur nanocolloid and SPECT/CT. *J Nucl Med* 2011; **52**: 1068–72.

- Li L, Mori S, Kodama M, Sakamoto M, Takahashi S, Kodama T. Enhanced sonographic imaging to diagnose lymph node metastasis: importance of blood vessel volume and density. *Cancer Res* 2013; **73**: 2082–92.
- Liao LJ, Lo WC, Hsu WL, Wang CT, Lai MS. Detection of cervical lymph node metastasis in head and neck cancer patients with clinically N0 neck—a meta-analysis comparing different imaging modalities. *BMC Cancer* 2012; **12**: 236.
- Kuhn FP, Hullner M, Mader CE *et al.* Contrast-enhanced PET/MR imaging versus contrast-enhanced PET/CT in head and neck cancer: how much MR information is needed? *J Nucl Med* 2014; **55**: 551–8.

- 7 Nathanson SD, Shah R, Chitale DA, Mahan M. Intraoperative clinical assessment and pressure measurements of sentinel lymph nodes in breast cancer. *Ann Surg Oncol* 2014; **21**: 81–5.
- 8 Garmy-Susini B, Avraamides CJ, Desgrosellier JS *et al*. PI3K α activates integrin $\alpha 4\beta 1$ to establish a metastatic niche in lymph nodes. *Proc Natl Acad Sci USA* 2013; **110**: 9042–7.
- 9 Cairns RA, Hill RP. Acute hypoxia enhances spontaneous lymph node metastasis in an orthotopic murine model of human cervical carcinoma. *Cancer Res* 2004; **64**: 2054–61.
- 10 Hompland T, Ellingsen C, Ovrebo KM, Rofstad EK. Interstitial fluid pressure and associated lymph node metastasis revealed in tumors by dynamic contrast-enhanced MRI. *Cancer Res* 2012; **72**: 4899–908.
- 11 Rofstad EK, Tunheim SH, Mathiesen B *et al*. Pulmonary and lymph node metastasis is associated with primary tumor interstitial fluid pressure in human melanoma xenografts. *Cancer Res* 2002; **62**: 661–4.
- 12 Shao L, Mori S, Yagishita Y *et al*. Lymphatic mapping of mice with systemic lymphoproliferative disorder: usefulness as an inter-lymph node metastasis model of cancer. *J Immunol Methods* 2013; **389**: 69–78.
- 13 Shao L, Ouchi T, Sakamoto M, Mori S, Kodama T. Activation of latent metastases in the lung after resection of a metastatic lymph node in a lymph node metastasis mouse model. *Biochem Biophys Res Commun* 2015; **460**: 543–8.
- 14 Shao L, Takeda K, Kato S, Mori S, Kodama T. Communication between lymphatic and venous systems in mice. *J Immunol Methods* 2015; **424**: 100–5.
- 15 Kodama T, Hatakeyama Y, Kato S, Mori S. Visualization of fluid drainage pathways in lymphatic vessels and lymph nodes using a mouse model to test a lymphatic drug delivery system. *Biomed Opt Express* 2015; **6**: 124–34.
- 16 Kato S, Shirai Y, Kanzaki H, Sakamoto M, Mori S, Kodama T. Delivery of molecules to the lymph node via lymphatic vessels using ultrasound and nano/microbubbles. *Ultrasound Med Biol* 2015; **41**: 1411–21.
- 17 Kodama T, Tomita N, Yagishita Y *et al*. Volumetric and angiogenic evaluation of antitumor effects with acoustic liposome and high-frequency ultrasound. *Cancer Res* 2011; **71**: 6957–64.
- 18 Li L, Mori S, Sakamoto M, Takahashi S, Kodama T. Mouse model of lymph node metastasis via afferent lymphatic vessels for development of imaging modalities. *PLoS ONE* 2013; **8**: e55797.
- 19 Nathanson SD, Mahan M. Sentinel lymph node pressure in breast cancer. *Ann Surg Oncol* 2011; **18**: 3791–6.
- 20 Okuno T, Kato S, Hatakeyama Y *et al*. Photothermal therapy of tumors in lymph nodes using gold nanorods and near-infrared laser light. *J Control Release* 2013; **172**: 879–84.
- 21 Don DM, Anzai Y, Lufkin RB, Fu YS, Calcaterra TC. Evaluation of cervical lymph node metastases in squamous cell carcinoma of the head and neck. *Laryngoscope* 1995; **105**: 669–74.
- 22 Hanahan D, Weinberg RA. Hallmarks of cancer: the next generation. *Cell* 2011; **144**: 646–74.
- 23 Swartz MA, Lund AW. Lymphatic and interstitial flow in the tumour microenvironment: linking mechanobiology with immunity. *Nat Rev Cancer* 2012; **12**: 210–9.
- 24 Matsumura Y, Maeda H. A new concept for macromolecular therapeutics in cancer chemotherapy: mechanism of tumorotropic accumulation of proteins and the antitumor agent smancs. *Cancer Res* 1986; **46**: 6387–92.
- 25 Liu D, Mori A, Huang L. Role of liposome size and RES blockade in controlling biodistribution and tumor uptake of GM1-containing liposomes. *Biochim Biophys Acta* 1992; **1104**: 95–101.
- 26 Yoon YS, Murayama T, Gravereaux E *et al*. VEGF-C gene therapy augments postnatal lymphangiogenesis and ameliorates secondary lymphedema. *J Clin Invest* 2003; **111**: 717–25.
- 27 Enholm B, Karpanen T, Jeltsch M *et al*. Adenoviral expression of vascular endothelial growth factor-C induces lymphangiogenesis in the skin. *Circ Res* 2001; **88**: 623–9.
- 28 Bouta EM, Wood RW, Brown EB, Rahimi H, Ritchlin CT, Schwarz EM. In vivo quantification of lymph viscosity and pressure in lymphatic vessels and draining lymph nodes of arthritic joints in mice. *J Physiol* 2014; **592**: 1213–23.

Supporting Information

Additional supporting information may be found in the online version of this article:

Table S1. Primer sequences used in this study.